



# Influence of Stress and Water Pressure on the Permeability of Fissured Sandstone Under Hydromechanical Coupling

Shuai Zhang<sup>1</sup> · Dongsheng Zhang<sup>1</sup> · Zhen Wang<sup>1</sup> · Mingwei Chen<sup>1</sup>

Received: 21 August 2017 / Accepted: 29 March 2018 / Published online: 9 April 2018  
© Springer-Verlag GmbH Germany, part of Springer Nature 2018

## Abstract

We investigated the permeability of fissured sandstone in the Lao Sangou coal mine to understand how to reduce water seepage through the mine roof and to provide a scientific basis for how the permeability changes. First, the physical and mechanical parameters of the sandstone samples were measured in laboratory tests. The discrete element method was used to establish a corresponding model, which was calibrated using uniaxial compression tests. Then, five calculation models were established and used to analyse the permeability of fissured sandstone at varied axial pressures, confining pressures, and water pressures under hydromechanical coupling. A further triaxial seepage experiment was carried out to test the permeability of the fissured sandstone samples. The results indicated that a horizontal hydraulic aperture was more sensitive to axial stress than a vertical hydraulic aperture, and that a vertical hydraulic aperture was more sensitive to confining stress than a horizontal hydraulic aperture, suggesting that confining stress affects permeability more than axial stress. Changes in permeability occur in three stages, i.e. slowly declining, sharply declining, and steady state, reacting to water pressure and stress. There is a cubic polynomial relationship between both the average flow rate and the average hydraulic aperture and stress, with  $R^2 \geq 0.95$ . After the permeability traverses the slowly declining stage, an exponential relationship exists between both the average flow rate and the average hydraulic aperture and stress, with  $R^2 \geq 0.97$ . A series of numerical calculation models were used to suggest a partition scheme, in which water pressure plays a leading role in zone I, the stress and water pressure work together in zone II, and stress plays a dominant role in zone III.

**Keywords** Coal mining · Water seepage · Discrete element method · Triaxial seepage experiment

## Introduction

Many methods have been used to study the permeability of rock, including field measurements, triaxial seepage experiments, and numerical simulation. Field measurements of rock permeability are usually reliable. However, these methods are not widely used due to the complexity of the geological environment, repeated mining disturbances, and the expensive testing required. Instead, most rock sample permeability tests are carried out in a laboratory. In

recent years, the permeability evolution of rock during the stress–strain process has been extensively investigated. Zhu and Wong (1997) carried out a triaxial seepage experiment with porous sandstone to analyse the influence of stress and failure modes on the axial permeability of sandstone with confining pressures ranging from 13 to 550 MPa and a pore pressure of 10 MPa. Their results indicated that permeability and stress are highly related. Wang and Park (2002) studied permeability evolution during the entire stress–strain process for sedimentary rocks, and found that permeability decreases with increased stress before the peak strength is reached, and that the permeability also decreases significantly during the strain softening stage. Worthington (2008) analysed the relationship between axial permeability and the effective stress of a sample, and determined that the relationship between the two could be described with a cubic polynomial function. Davies and Davies (1999) studied the permeability stress sensitive characteristics of different cores. Their results indicate that the greater porosity and permeability of

**Electronic supplementary material** The online version of this article (<https://doi.org/10.1007/s10230-018-0540-2>) contains supplementary material, which is available to authorized users.

✉ Dongsheng Zhang  
dshzhang123@126.com

<sup>1</sup> State Key Laboratory of Coal Resources and Safe Mining, School of Mines, China University of Mining and Technology, Xuzhou 221116, China

a sandstone core, and the lesser permeability of a cementitious low-permeability sandstone core, correspond to greater stress sensitivity. Wu et al. (2005) carried out CT scans and real-time observations during a seepage-stress coupling test of sandstone, and studied the relationship between the porosity and permeability of sandstone on a mesoscopic scale. They found that permeability increased with the occurrence of micro-cracks, and that it peaked after a macroscopic failure occurred. Yu et al. (2013) conducted triaxial servo-testing of rock with varied confining and osmotic pressures, and determined that the permeability change curve demonstrated three trends: increasing, flat, and decreasing.

Numerical simulation methods are increasingly used for permeability testing of fissured rocks. Baghbanan and Jing (2007) used discrete fracture network models of varied sizes and trace lengths to simulate the effects of fracture aperture and trace length on the permeability of fractured rock. Li et al. (2016) established a series of numerical models to study the permeability of concrete. Indraratna (1995) and Wang (2000) combined a fracture network model with the discrete element method to analyse the seepage-stress coupling process and establish a seepage-stress coupling model that incorporates the seepage flow of the rock mass. Kim et al. (1999) and Jing et al. (2001) studied the seepage-stress coupling of a rock mass during excavation with a discontinuous deformation analysis. Blesent et al. (2009) used geological modelling in combination with numerical modelling to calculate the seepage field of a three-dimensional fractured rock mass. Cammarata et al. (2007), Cappa et al. (2004), and Guglielmi et al. (2008) carried out numerical studies of seepage-stress coupling using boundary element, discontinuous element, and continuous element methods, respectively.

A discrete element numerical model of hydromechanical coupling was therefore established. Numerical calculations for a fractured rock mass were applied to establish a model based on the naturally occurring complex geometry of fractures and the contact interactions between rock blocks (Lemos and Lorig 1990; Min and Jing 2003). A triaxial seepage-stress coupling test using an automatic three-axis servo was also carried out to evaluate the effects of varied stresses and water pressures on the contact hydraulic aperture, seepage channel, and average flow rate.

## Sample Extraction

The Lao Sangou coal mine is located in the northeastern part of Ordos, which is a typical loess plateau. This area is covered by loess and aeolian sand. It was necessary to determine the physical and mechanical parameters and permeability of the sandstone roof of coal mine #6, which is in the Lao-sangou coal seam. First, geological boreholes were drilled

into the Lao Sangou mine to extract rock samples (see supplemental Fig. 1). This study focused primarily on investigating a 26 m thick gravel sandstone at a depth of 456 m. Samples were packaged after extraction to reduce the influence of external factors on their physical and mechanical properties. Indoor processing and experiments were carried out in a timely fashion. Physical and mechanical properties that were measured included tensile strength, compressive strength, shear strength, internal friction angle, cohesion, permeability, and porosity, all of which provide the information required for further study of the relationship between the stress, water pressure, and permeability.

## Numerical Simulation Using Discrete Element Modelling

The Universal Distinct Element Code (UDEC) is a tool that uses a problem-solving program to provide effective and accurate analyses for geotechnical engineering. It is particularly suitable for analysing the response of a jointed rock system, as well as for the collection system of a discontinuous block under a static plate or power loading (Zhang et al. 2017). It is widely used in geotechnical fields and has been successfully used in numerous applications for studies on rock failure and development of rock fractures.

### Contact Constitutive Model

Multiple studies have shown that the 2D Voronoi model in UDEC can reliably simulate mechanical responses for both laboratory tests of rock and field observations (Abdollahipour et al. 2016; Damjanac and Fairhurst 2010; Gao 2013; Kazerani et al. 2012). Both deformable and rigid polygon blocks can be produced in UDEC; the polygon blocks cannot be destroyed, and a fracture can only be generated along the edges of a polygon. The generated polygon blocks are connected by joints, and the relationship between the force and displacement at these joints is determined based on the normal joint stiffness and shear stiffness. The strength of a joint depends on the cohesion, internal friction angle, and tensile strength of the joint (Nicksiar 2013). The joints break when the stress between polygons is greater than the shear and tensile stress limits the joint can withstand. Therefore, the initiation, expansion, and closure of the joints between polygons can be used to simulate the fracture generation processes (see supplemental Fig. 2; Lisjak and Grasselli 2014).

UDEC can be used to simulate the flow of a fluid in a rock joint under a static load; the blocks in the model are impermeable, and the fluid can only flow at the joints (Itasca 2011; Fig. 1). The fluid flow rate between the planar surfaces during contact is given by:

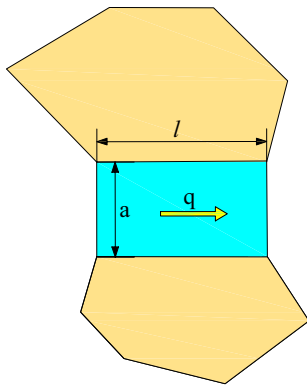


Fig. 1 the fluid flow rate of contact

$$q = \frac{ba^x \Delta p}{12\mu l}, \tag{1}$$

where  $a$  is the fracture width (aperture),  $b$  is an empirical coefficient,  $\mu$  is the viscosity of the fluid,  $x$  is the aperture exponent,  $l$  is the length of the contact between domains, and  $\Delta p$  is the pressure between the domains. The most widely used form of this relation is the cubic flow law, i.e.  $x=3$  and  $b=1$ .

During the simulation process, mechanical deformation affects the contact hydraulic aperture. These effects are modelled in UDEC and are summarised in Fig. 2, where the contact hydraulic aperture is given by:

$$a = a_0 + \Delta a \tag{2}$$

$$\Delta a = \frac{\sigma_n}{k_n} \tag{3}$$

where  $a_0$  is the aperture under zero normal stress,  $\sigma_n$  is the normal stress at the contact,  $k_n$  is the contact normal stiffness, and  $a_{res}$  is the residual aperture at high stress. As the stress increases, the residual aperture width decreases until it reaches the minimum aperture value, at which point mechanical deformation does not affect contact permeability.

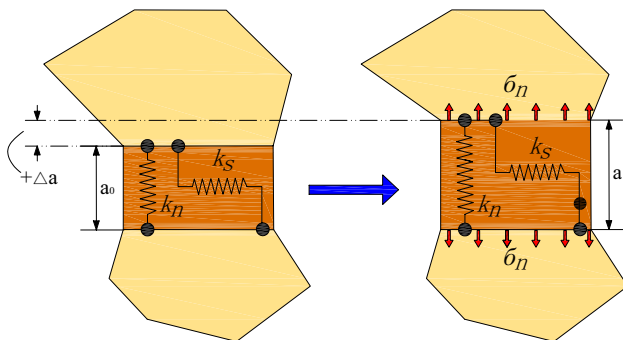


Fig. 2 the contact hydraulic aperture

### Calibration of Rock Properties

Given the inherent advantages of UDEC for simulating fracture development in rock, the mechanism of internal fracture development was observed in this study using discrete element modelling (DEM; Zhang et al. 2016). A 2D numerical model was established with UDEC to simulate the response of rock under uniaxial compression. The model has dimensions of 100 mm × 50 mm (height × width). The model was divided into polygonal Voronoi cells using the Voronoi tessellation generator command to set the number of seeds, which usually have a relatively uniform grain size (Li et al. 2006; Nygard and Gudmundson 2002), as shown in Fig. 3.

To ensure that the established numerical model can effectively represent the mechanical behaviour of rock, reasonable physical mechanics parameters need to be determined for the model. From Eqs. (1)–(3), it can be seen that the contact hydraulic aperture significantly affects the relationship between fluid flow and stress in the DEM model for coupled mechanical-hydraulic simulations. The rock’s fracture characteristics not only determine its seepage characteristics, but also affect its mechanical properties (Ni et al. 2017; Xie and Chen 1989). A scanning electron microscope (SEM) was used to analyse the rock samples extracted from the Lao Sangou mine, and to provide data on the characteristics of the pores, fracture morphology, and fracture sizes of the rock mass (see supplemental Fig. 3), which were then applied to the numerical model. The fracture widths at zero stress were 6.4, 5.5, 5.1, and 7.2 μm. The value for the aperture at zero normal stress used in the model was the mean of the four values above,  $a_0=6 \mu\text{m}$ . The mechanical parameters

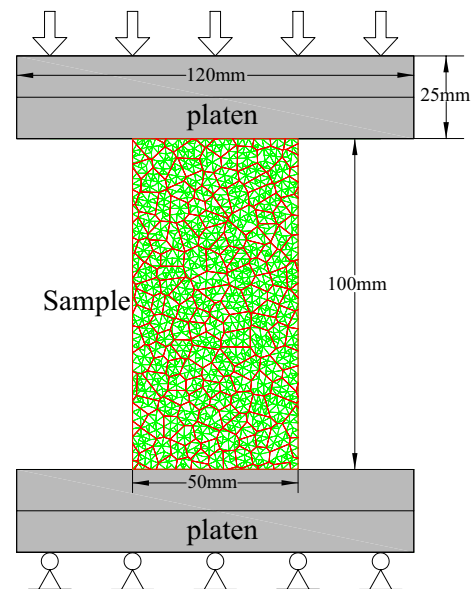


Fig. 3 Numerical model of uniaxial compression tests

obtained from the laboratory tests can be used to calculate the area according to Eqs. (1)–(3).

The mechanical parameters used in the model are summarized in Table 1. A previously published method (Bai et al. 2016; Gao and Stead 2014) was used to fit the uniaxial compressive strength of the rock in this study and determine the mechanical parameters for the blocks and contacts in the model. Figure 4 shows the experimental and numerical simulation results for the uniaxial compression tests. A slope failure on the surface occurred throughout the specimen when the rock sample was damaged (Fig. 4a). The same failure mode was also obtained in the numerical simulations (Fig. 4b, c). Figure 4d shows a stress–strain curve for the sample. The peak stress for the uniaxial compression was 52.38 MPa. Before reaching the peak, the stress increased linearly with increasing strain. After the peak, the stress then decreased rapidly. To ensure that the contacts in the model were not damaged, the maximum stress applied in the model did not exceed 40 MPa. The numerical simulation results for the uniaxial compression fit the experimental results well, indicating that the mechanical parameters for the blocks and contacts used in the model were reasonable.

### Flow Model Establishment

Five numerical models were used in this study (Fig. 5). Models 1, 2, and 3 shared some boundary conditions, including a fixed lower boundary, impermeable left and right boundaries, and P1 and P2 of 0 and 2 MPa, respectively. The differences in the boundary conditions for these three models include: 5–40 MPa of axial stress applied to the upper boundary of Model 1; 5–30 MPa of confining stress applied to the left and right boundaries of Model 2; and 5–40 MPa of axial stress and 5–30 MPa of confining stress applied to Model 3. Shared boundary conditions for Models 4 and 5 included a fixed lower boundary, impermeable left and right boundaries, and P1 and P2 of 1–8 and 0 MPa, respectively. The boundary condition differences between the two models included: 5–40 MPa of axial stress and 10 MPa of confining stress applied to model 4; and 10 MPa of axial stress and 5–30 MPa of confining stress applied to model 5. To reduce the impact of accidental factors, each model condition was simulated at least five times.

This study was primarily focused on the effects of stress and water pressure on permeability after the rock mass has reached saturation. Therefore, only a steady-state fluid flow was used in this study. Three methods were used to determine whether the seepage in the contact had reached a balance. (a) When entering ‘print Max’ in the UDEC command window, if ‘inflow’ is equal to ‘outflow’, the joint seepage is balanced. (b) The pore pressures of all contacts in the model were monitored (see supplemental Fig. 4a, c), and when the pore pressure in the joint

**Table 1** Calibration mechanical properties of the sample used in the numerical model

UCS	Young's modulus	Poisson's ratio
Material properties		
53.6 MPa	8.289 GPa	0.27
Block Young's modulus		
8.289 GPa	6100 GPa	0.25
Calibrated micro-parameters		
Joint friction	Joint normal stiffness	Joint shear stiffness
22°	6e <sup>-6</sup> m	2440 GPa
	Joint tension	Joint cohesion
	6.9 MPa	22.4 MPa
		Residual hydraulic aperture
		3e <sup>-7</sup> m

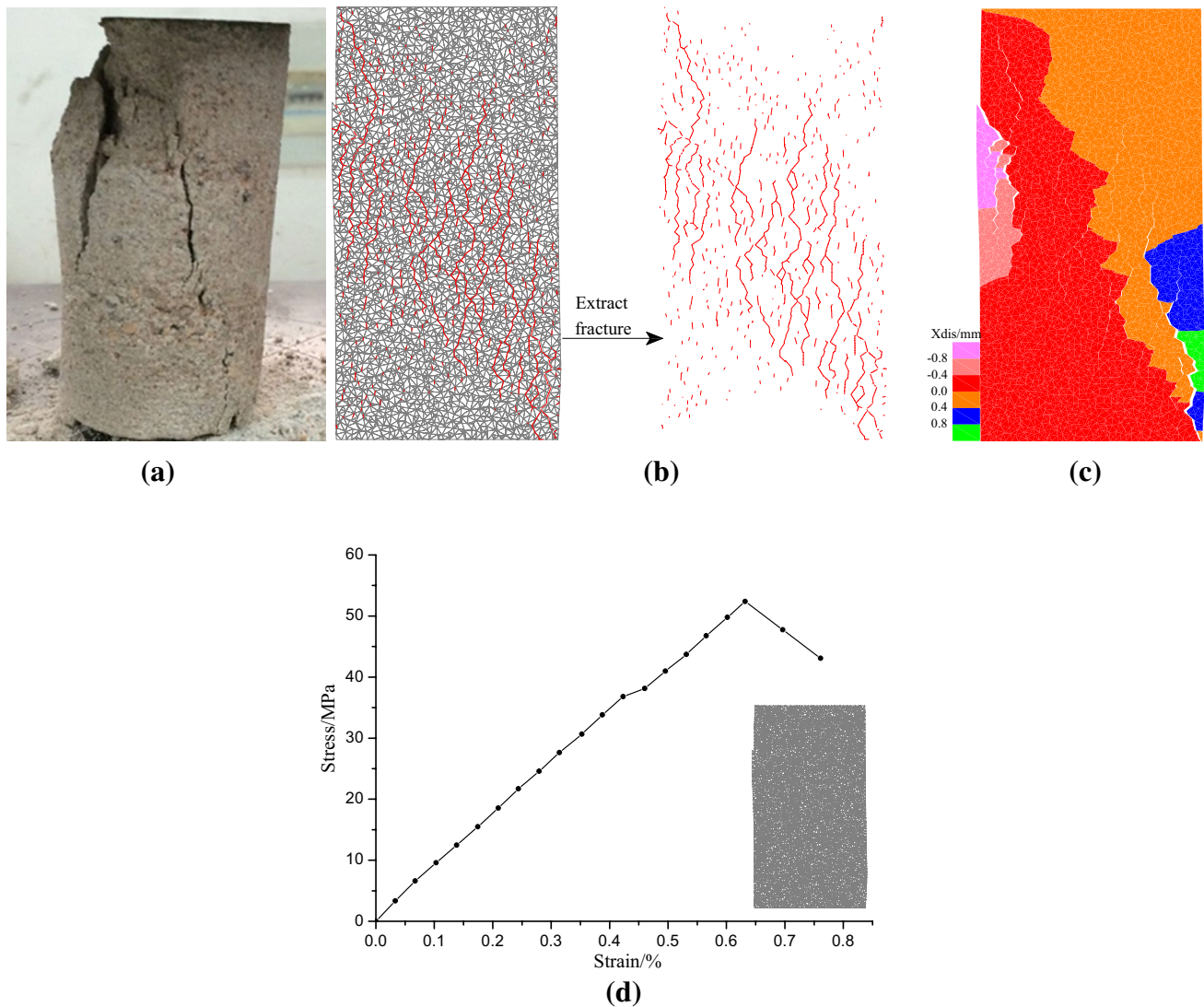


**Fig. 4** Calibration of numerical model to uniaxial compression tests, **a** failure pattern of laboratory sample, **b** failure pattern of numerical model, **c** xdis of numerical model, **d** stress–strain curve of numerical model

no longer changed, the joint seepage was determined to have reached equilibrium. The models with 5, 10, and 15 MPa of axial stress reached a steady state after 3,250 steps, while the models with 20, 25, 30, 35, and 40 MPa of axial stress reached a steady state after 4500, 12,500, 23,500, 30,450, and 35,500, steps, respectively. The steps required for the seepage to reach equilibrium increased with increasing axial stress. The models with 5 and 10 MPa of confining stress reached steady state after 3000 steps, whereas the models with 15, 20, and 25 MPa of confining stress reached steady state after 5900, 39,000, and 58,500 steps, respectively, and the model with 30 MPa of confining stresses had nearly reached a steady state after 73,500 steps. The steps required for the seepage to reach equilibrium under different stresses were recorded, and the results provided guidance and reference for the selection

of time steps in subsequent numerical models. (c) When the seepage has reached equilibrium, the pore pressure of the contact presents an evenly distributed layer (see supplemental Fig. 4b, d). The ‘print max’ command was used in UDEC to list the maximum and average flow rates and the average contact hydraulic aperture.

Models 1 and 2 were used to study the effects of axial stress and confining stress on the permeability and seepage of the channels. In these cases, the axial stress was parallel to the seepage direction, and the confining stress was perpendicular to the seepage direction, allowing the effects of stress direction on permeability to also be investigated. Model 3 was used to analyse the effects of varied stresses on the permeability. Finally, Models 4 and 5 were used to study the seepage law under different osmotic pressures.



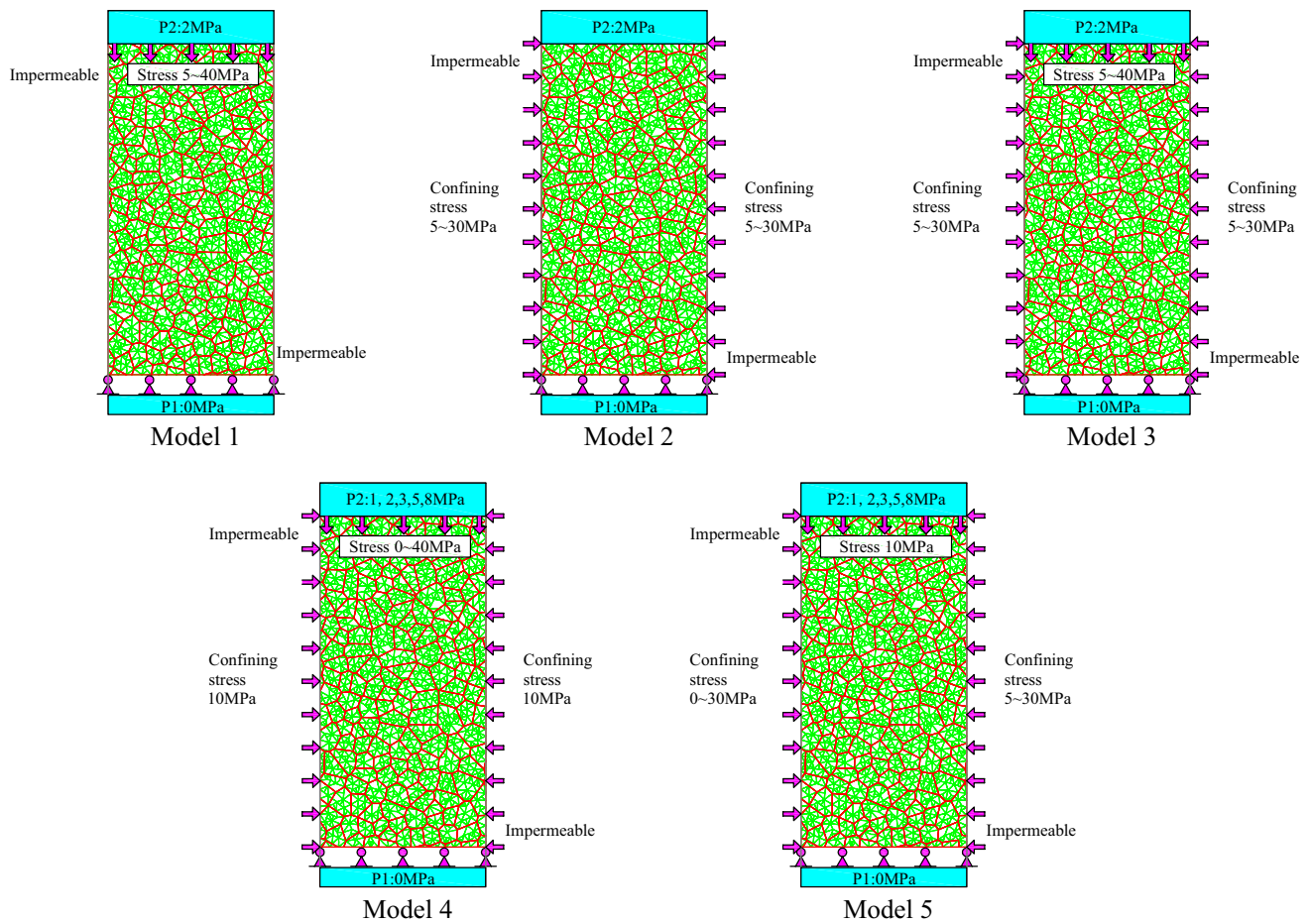


Fig. 5 Flow numerical calculation model

### Simulation Results for Models

For a more detailed description of the models and analysis of the simulation results, please see the supplemental simulation results for models.docx, which accompanies the on-line version of this paper, along with all of the other supplemental files.

The simulation results for models 1, 2, and 3 show that with an increase in axial stress, the hydraulic aperture for a horizontal contact gradually closed, while there was no clear change in hydraulic aperture for a vertical contact (Fig. 6). The main seepage channel changes from mesh-like into a “*chuan*” (worm-like in appearance) channel, and the seepage channels are mainly composed of vertical

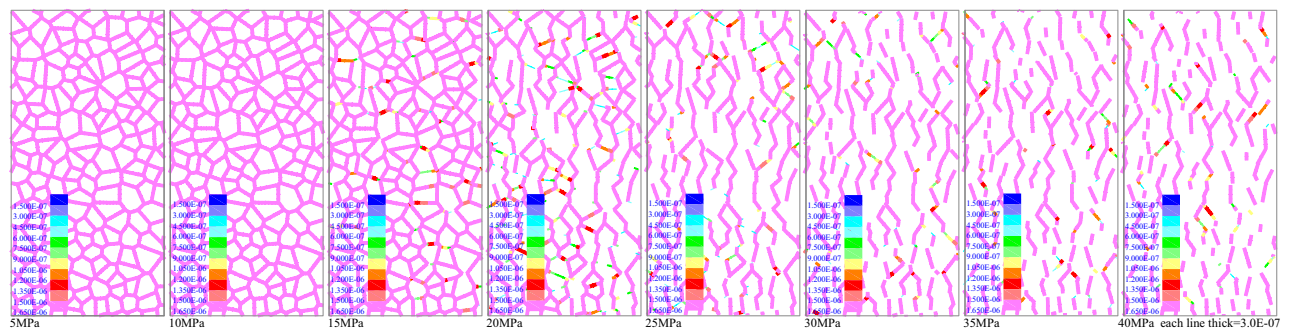
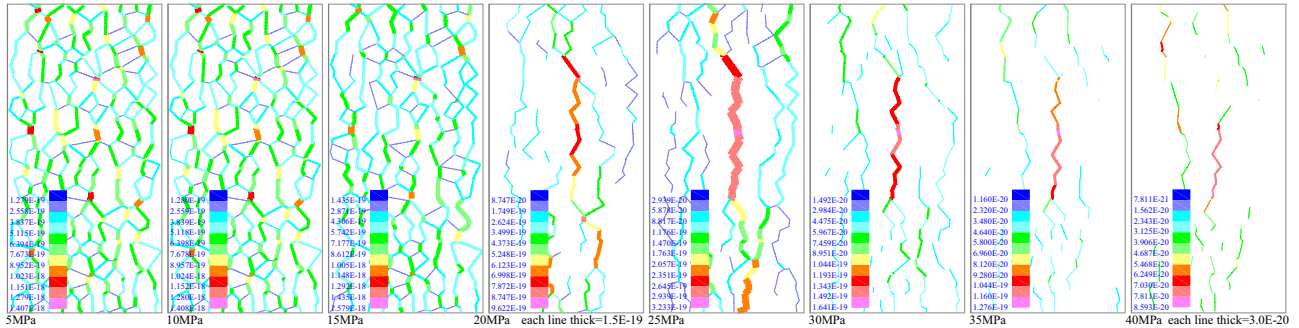


Fig. 6 Contact hydraulic aperture of the model 1 under different axial stress

contacts, with only a small number of horizontal contacts (Fig. 7). With increasing confining stress, the vertical contact hydraulic aperture gradually closes. While there was no clear change in the horizontal contact hydraulic aperture, the horizontal contact tends to expand when the

stress is high (Fig. 8). The main seepage channel changes from mesh-like into a z-shaped channel, and the seepage channels are primarily composed of horizontal and oblique contacts, with only a small number of vertical contacts (Fig. 9).



**Fig. 7** Contact flow rate and main seepage channel of the model 1 under different axial stress

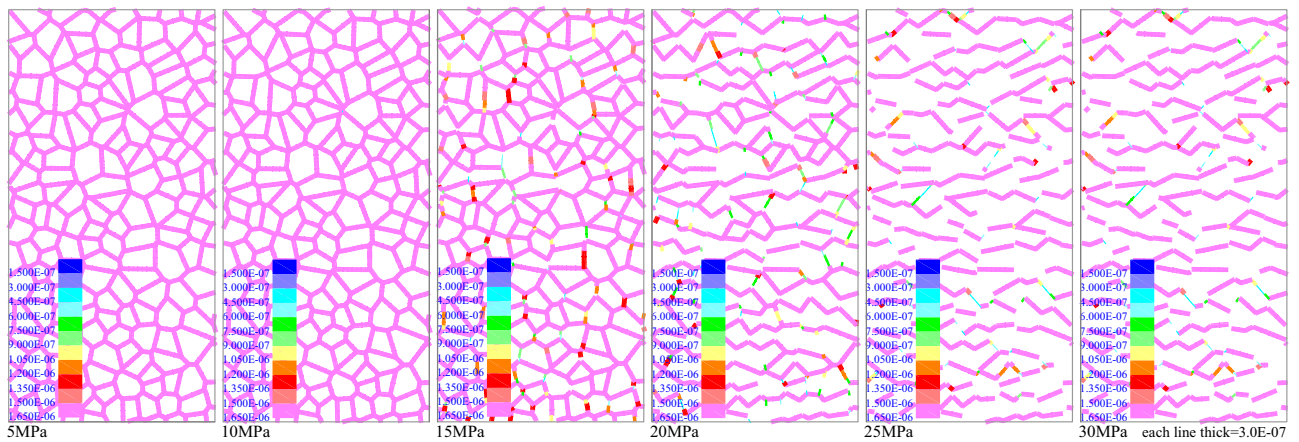


**Fig. 8** Contact hydraulic aperture of the model 2 under different confining stress

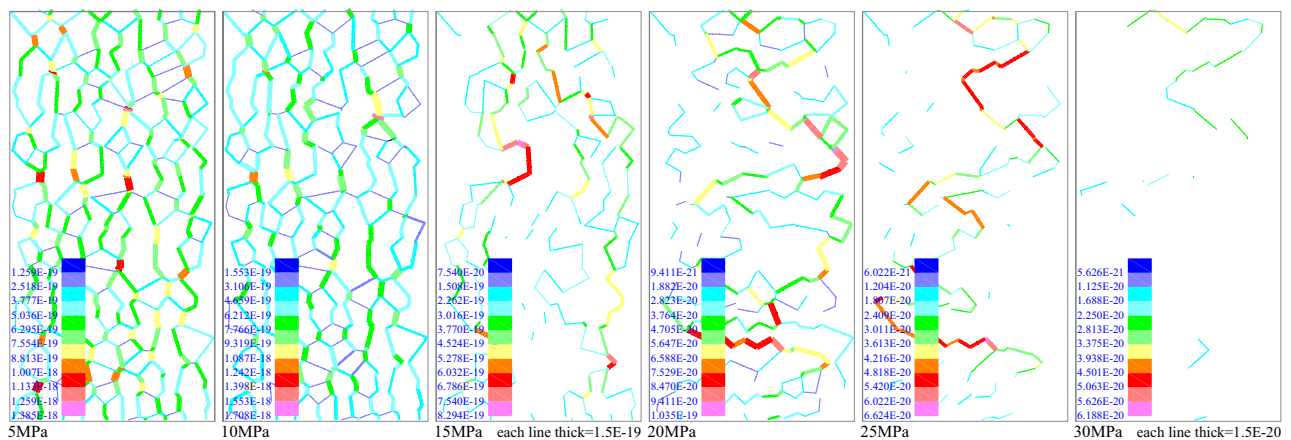


**Fig. 9** Contact flow rate and main seepage channel of the model 1 under different confining stress

When the confining stress is less than 10 MPa, the flow rate change curves can be divided into three stages: a slowly declining stage (axial stress of 5–10 MPa), a sharply declining stage (axial stress of 10–25 MPa), and a steady state stage (axial stress of 25–40 MPa). When the confining stress is 10–20 MPa, the contact hydraulic aperture decreases significantly (Fig. 10b), resulting in a sharp decline in the contact flow rate (Fig. 10a). This creates an interesting phenomenon: the change curves of the flow rate transitions from having three stages to having only two stages (a sharply declining stage, with an axial stress of 0–15 MPa, and a steady stage, with an axial stress of 15–40 MPa (Fig. 10a). When the confining stress is more than 20 MPa, the change

in the contact flow rate clearly decreases and tends to stabilize. The simulation results for model 4 and model 5 indicate that there is a linear relationship between the flow rate and the water pressure (Figs. 11b, 12b). When the axial stress is 0–10 MPa, the osmotic pressure plays a major role, while the effect of the axial pressure is unclear. When the axial stress is 10–20 MPa, the flow rate drops sharply because many of the horizontal contact hydraulic apertures begin to reach the residual value and some of the seepage channels close (see supplemental Fig. 5b). When the axial stress exceeds 20 MPa, the effect of the osmotic pressure on the joint seepage decreases sharply, and the effect of increasing water pressure on the change in flow rate is unclear, as shown

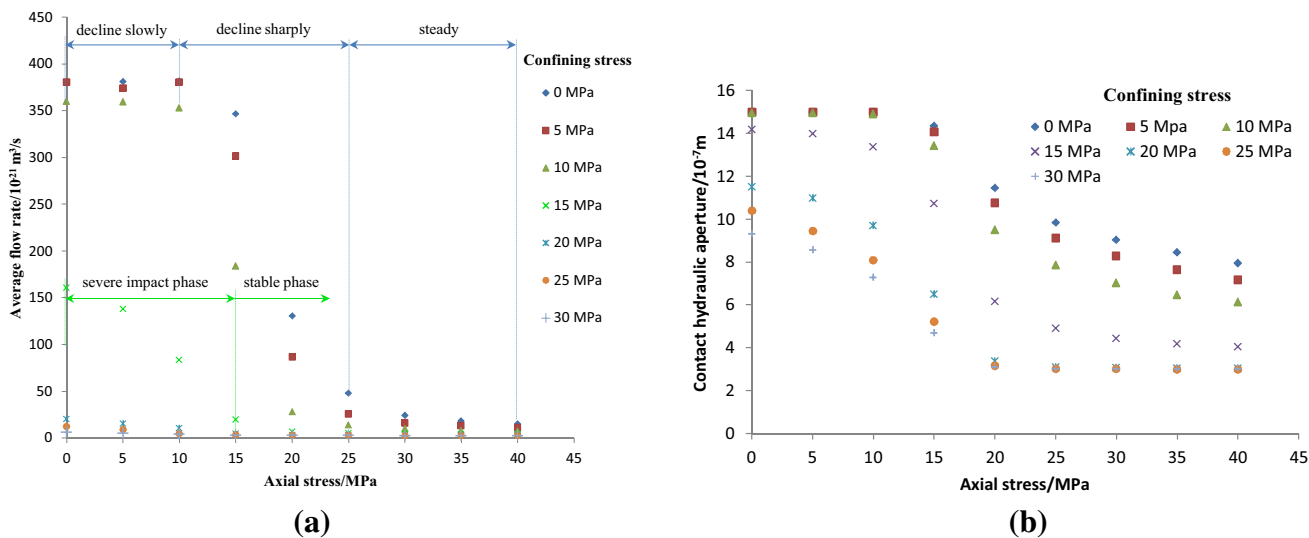


Fig. 10 The simulation results of the model 3 a the flow rate change curves of the model 3, b the flow rate and contact hydraulic aperture change curves of the model 3

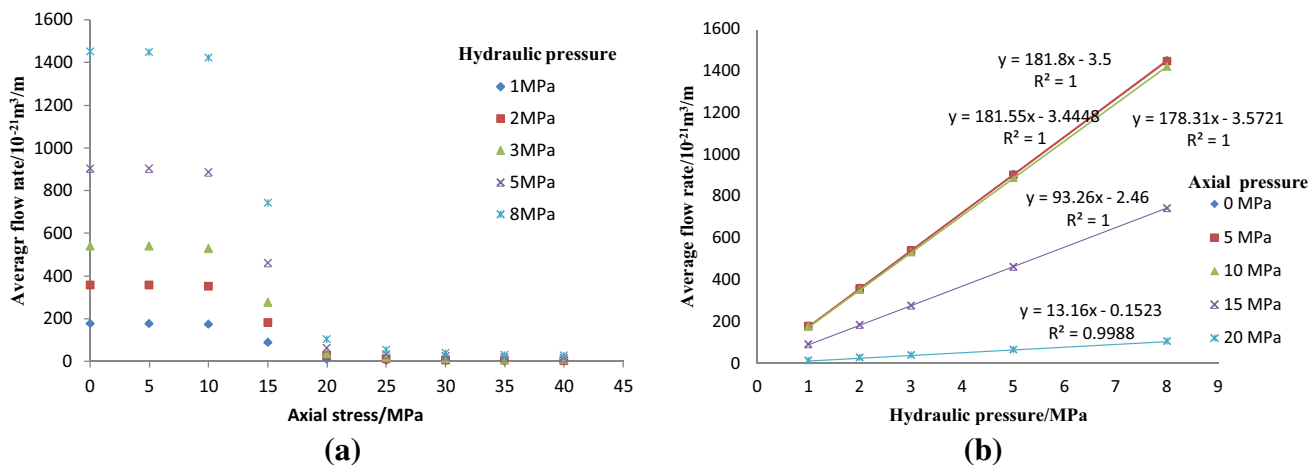
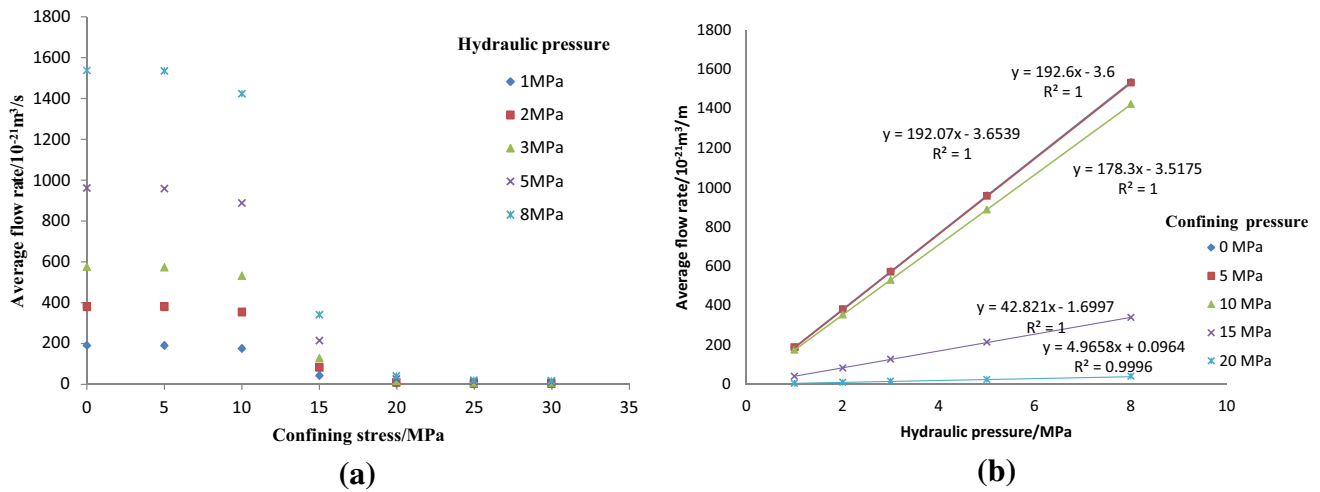


Fig. 11 The flow rate change curves of the model 4 a the relationship between flow rate and axial stress, b the relationship between flow rate and hydraulic pressure





**Fig. 12** The flow rate change curves of the model 5 **a** the relationship between flow rate and confining stress, **b** the relationship between flow rate and hydraulic pressure

in Fig. 11a. When the confining stress is 0–10 MPa, the osmotic pressure plays a significant role, while the effect of the confining pressure is unclear. When the confining stress is 10–20 MPa, the flow rate decreases sharply because a large number of vertical hydraulic contact apertures begin to reach the residual value and a number of seepage channels are closed (see supplemental Fig. 5d). When the confining stress is greater than 20 MPa, the effect of the osmotic pressure on the joint seepage decreases sharply, as shown in Fig. 12a.

An additional 140 numerical models were executed to examine the average change in flow rate for samples with axial stresses of 5 and 15–40 MPa, confining stresses of 5 and 15–30 MPa, and osmotic pressures of 1, 3, 5, and 8 MPa. The flow rate change at 1, 3, 5, and 8 MPa is similar to that at 2 MPa. Three regions (I, II, and III) were obtained,

with the average flow rate as the primary index (Fig. 13). In region I, the average flow rate was approximately constant with increasing stress, and increased linearly with increasing osmotic pressure at slopes of  $178^\circ$ – $192^\circ$ , indicating that osmotic pressure plays a major role in determining the contact seepage. In region II, the average flow rate decreased sharply with increasing stress, and increased linearly with increasing osmotic pressure at slopes of  $42^\circ$ – $93^\circ$ . Compared to region I, the linear slopes were reduced, indicating that the effect of osmotic pressure was also reduced. In region III, the average flow rate was approximately stable with increasing stress, and increased linearly with increasing osmotic pressure at slopes of  $4^\circ$ – $12^\circ$ . Compared to regions I and II, the osmotic pressure showed only a weak effect on joint seepage because, in this region, almost all of the hydraulic contact apertures have reached the residual value under the

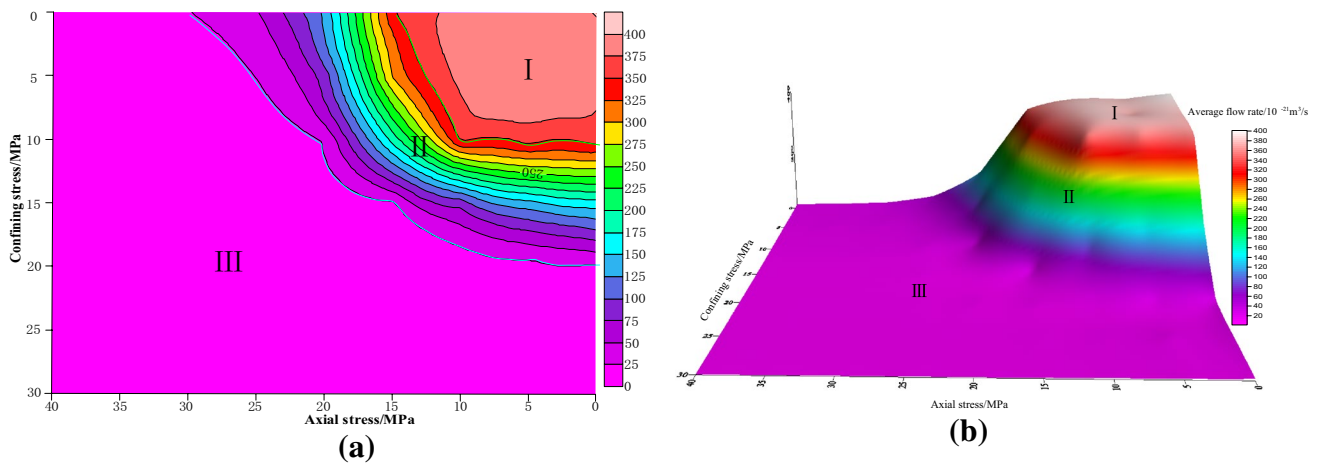


**Fig. 13** The partition according to the contact flow rate, **a** the plan, **b** the stereogram

action of the stress. For the same osmotic pressure (1, 2, 3, 5, or 8 MPa), when the axial pressure increased from 10 to 15 MPa, the linear slope decreased by 47.7%, from 178.3° to 93.3°, as shown in Fig. 11b. When the confining pressure increased from 10 to 15 MPa, the linear slope decreased by 76%, from 178.3° to 42.8°, as shown in Fig. 12b. These results indicate that confining stress has a more significant impact on permeability than axial stress.

### Triaxial Seepage Experiment

An experiment was carried out using the MTS 815.02 electro-hydraulic servo rock mechanics triaxial seepage test system at the Central South University Mechanics Laboratory. This system consists of three separate loading systems (confining pressure, axial pressure, and water pressure), and has full digital computer control and automatic data collection functionalities, which allows it to be used for rock mechanics tests of stress-seepage coupling. An image and a schematic diagram of the test system are shown in supplemental Fig. 8. A flow chart of the algorithm representing the experimental process for the permeability stress test is shown in supplemental Fig. 9. The three separate loading systems applied a designated axial pressure, P1, confining pressure, P2, and water pressure, P3, to the sample. The water pressure at one end of the sample was then reduced (P4) to provide an osmotic pressure difference between the two ends of the sample, resulting in water flow through the sample to produce seepage. The above procedure was applied in a loop, and P2 and P3 were then adjusted to execute the next cycle until the end of the test.

Rock samples from the Lao Sangou mine were used for the triaxial seepage experiment. During the experiment, the osmotic pressure difference in the sample was  $\Delta P=2$  MPa; the confining pressure was set to 5, 10, or 15 MPa and the axial pressure was set to 0, 5, 10, 15, 20, 25, 30, 35, or 40 MPa. The results of these tests are shown in Fig. 14. The change curves for the permeability at 5 and 10 MPa of confining pressure can be divided into three stages: increasing axial pressure, i.e. a slowly declining stage (0–15 MPa); slightly decreased permeability, i.e. a sharply declining stage (15–25 MPa); and sharply reduced permeability, i.e. a steady stage (25–40 MPa), where the permeability is nearly stable. The change curves for the permeability at 15 MPa first increased and then sharply decreased, before finally stabilising with respect to increasing axial pressure. When the axial pressure increased from 10 to 15 MPa, the permeability at 5, 10, and 15 MPa of confining pressure decreased by  $9.2E-15$ ,  $3.92E-14$ , and  $2.60E-14$  cm<sup>2</sup>, respectively, with an average decrease in permeability of  $2.48E-14$  cm<sup>2</sup>. When the confining pressure increased from 10 to 15 MPa, the permeability at 5, 10, and 15 MPa of axial pressure decreased by

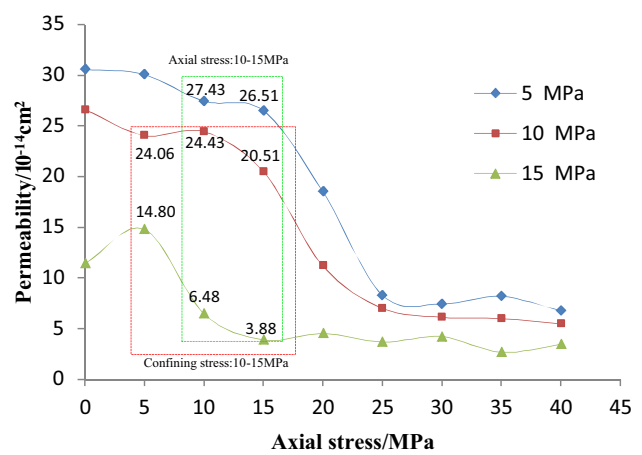


Fig. 14 The laboratory permeability testing result

$9.26E-14$ ,  $1.79E-13$ , and  $1.66E-13$  cm<sup>2</sup>, respectively, with an average decrease in permeability of  $1.46E-13$  cm<sup>2</sup>. These results show that confining pressure has a more significant influence on permeability than axial pressure. The permeability changed slightly during the early stages, and then it decreased sharply, before finally stabilising with respect to increased axial pressure. The numerical results agree well with the experimental results, and the experimental results provide a further validation of the numerical simulation.

### Discussion

In this study, UDEC models were used to investigate the effects of stress and water pressure on the contact hydraulic aperture, seepage channels, and contact flow rate at varied axial pressures, confining pressures, and water pressures. The DEM provides insight into how stress and water pressure influence the permeability of the fractured sandstone. Because the characteristics of fractures affect seepage and a rock’s mechanical properties, a SEM was used to characterize fracture development (see supplemental Fig. 3) in the rock samples; the results were incorporated into the numerical model.

Evidence suggests that fracture aperture and pore structure exert primary control on stress sensitivity, that stress and the main seepage channel both influence seepage characteristics, and that there are functional relationships (cubic polynomial, exponential, Gaussian function, etc.) between permeability and stress (Gale 1982; Jones 1975; McKee et al. 1988; Min et al. 2004; Worthington 2008). Our work revealed a cubic polynomial function relationship between both the average aperture and average flow rate and the stress (as shown in supplemental Fig. 5a, Fig. 6a).

An interesting phenomenon was found in the analysis, i.e. when the slowly declining stage is ignored, there is an

exponential function relationship between both the average aperture and average flow rate and the stress (see supplemental Fig. 5b and Fig. 6b). The numerical models suggest a partition into three regions. In region I, the average flow rates change slightly with increased stress, and the average flow rate increases linearly with an increase in osmotic pressure. This is because the contact hydraulic aperture does not significantly change in this stress environment. In region II, the average flow rate decreases sharply with increasing stress, and the average flow rate increases linearly, with increasing osmotic pressure. Compared to region I, the slope of the line was drastically reduced in region II because many of the contact hydraulic apertures had reached their residual value, causing the seepage channel to close due to the axial and confining pressures. In region III, the average flow rate was relatively stable with increasing stress, and the average flow rate increases linearly with increasing osmotic pressure. This is because almost all of the hydraulic contact apertures had reached their residual values, causing all of the seepage channels to close. Research results indicate that not only the size of the contact hydraulic aperture but also the direction of contact hydraulic aperture has important influence on the permeability of the fractured sandstone under the action of stress and water pressure. When the vertical contacts develop in the sample, the permeability increases. Comparatively speaking, when the horizontal contacts develop in the sample, the measured permeability decreases. This is important in preparing the samples and evaluating the permeability of the fractured rock mass using hydromechanical coupling tests.

## Conclusion

The discrete element method was used to establish a numerical model of hydromechanical coupling, and a triaxial seepage-stress coupling test was carried out to investigate the effects of stress and water pressure on permeability at varied axial pressures, confining pressures, and water pressures. The results indicate that with increasing axial stress, the horizontal contact hydraulic aperture gradually closes. The horizontal hydraulic aperture is more sensitive to axial stress than the vertical hydraulic aperture. The seepage channel is mainly composed of vertical contacts, with only a small number of horizontal contacts.

With increasing confining stress, the vertical contact hydraulic aperture gradually closes. The vertical hydraulic aperture is more sensitive to confining stress than the horizontal hydraulic aperture, and the seepage channels are mainly composed of horizontal and oblique contacts, with a small number of vertical contacts. The change curves for the flow rate are divided into three regions (slowly declining, sharply declining, and steady state) with the average flow

as the main index and the average hydraulic aperture as the auxiliary index. A cubic polynomial function can describe the relationship between both the average aperture and average flow rate and both the axial stress and confining stress, with  $R^2 \geq 95\%$ . In the slowly declining and steady stages of the curves, an exponential relationship occurs between both the average aperture and the average flow rate and both the axial stress and the confining stress, with  $R^2 \geq 97\%$ . Under the action of the same osmotic pressure (1, 2, 3, 5, or 8 MPa), when the axial pressure increases from 10 to 15 MPa, the linear slope decreases by 47.7%. In addition, when the confining pressure increases from 10 to 15 MPa, the linear slope decreases by 76%, indicating that the confining stress has a more significant impact on permeability than axial stress.

The numerical models suggest a partition into three regions: in zone I, the contact hydraulic aperture did not reach the residual value under the action of stress, and the osmotic pressure played a major role in determining the contact seepage. In zone II, a large amount of the contact hydraulic aperture reached the residual value, causing many of the seepage channels to close in response to the stress. As a result, the effect of the osmotic pressure was reduced, and the stress played a major role in determining the contact seepage. Finally, in zone III, almost all of the contact hydraulic aperture had reached their residual value, causing all seepage channels to close, and the osmotic pressure only weakly affected the contact seepage.

**Acknowledgements** The research was financially supported by the National Basic Research Program of China (2015CB251600), the Qing Lan Project (Grant Sujiaoshi (2016)15), the Jiangsu basic research program (Natural Science Foundation, BK20150051). We also thank the Lao Sangou Coal Mine for their support.

## References

- Abdollahipour A, Marji MF, Bafghi AY (2016) DEM simulation of confining pressure effects on crack opening displacement in hydraulic fracturing. *Int J Min Sci Technol* 26(4):557–561
- Baghbanan A, Jing L (2007) Hydraulic properties of fractured rock masses with correlated fracture length and aperture. *Int J Rock Mech Min* 44(5):704–719
- Bai QS, Tu SH, Zhang C (2016) Discrete element modeling of progressive failure in a wide coal roadway from water-rich roofs. *Int J Coal Geol* 167:215–229
- Blessent D, Therrien R, Macquarrie K (2009) Coupling geological and numerical models to simulate groundwater flow and contaminant transport in fractured media. *Comput Geosci* 35(9):1897–1906
- Cammarata G, Fidelibus C, Cravero M, Barla G (2007) The hydro-mechanically coupled response of rock fractures. *Rock Mech Rock Eng* 40(1):41–61
- Cappa F, Guglielmi Y, Fénart P, Merrien-Soukatchoff V, Thoraval A (2004) Hydromechanical interactions in a fractured carbonate reservoir inferred from hydraulic and mechanical measurements. *Int J Rock Mech Min* 42(2):287–306

- Damjanac B, Fairhurst C (2010) Evidence for a long-term strength threshold in crystalline rock. *Rock Mech Rock Eng* 43(5):513–531
- Davies JP, Davies DK (1999) Stress-dependent permeability: characterization and modeling. Proc, SPE Annual Technical Conf and Exhibition. <https://doi.org/10.2118/56813-MS>
- Gale JE (1982) The effects of fracture type (induced versus natural) on the stress-fracture closure-fracture permeability relationships. Proc, 23rd US Symp on Rock Mechanics, American Rock Mechanics Assoc. <https://www.onepetro.org/conference-paper/ARMA-82-290>
- Gao F (2013) Simulation of failure mechanisms around underground coal mine openings using discrete element modelling. PhD thesis, Simon Fraser Univ, Burnaby
- Gao FQ, Stead D (2014) The application of a modified Voronoi logic to brittle fracture modelling at the laboratory and field scale. *Int J Rock Mech Min* 68:1–14
- Guglielmi Y, Cappa F, Rutqvist J, Tsang CF, Thoraval A (2008) Mesoscale characterization of coupled hydromechanical behavior of a fractured-porous slope in response to free water-surface movement. *Int J Rock Mech Min* 45(6):862–878
- Indraratna B (1995) Hydromechanical aspects of jointed rock media. Proc, 8th ISRM Congress, International Soc for Rock Mechanics
- Itasca Consulting Group Inc (2011) UDEC: Universal Distinct Element Code, Version 5.0, ICG, Minneapolis
- Jing L, Ma Y, Fang Z (2001) Modeling of fluid flow and solid deformation for fractured rocks with discontinuous deformation analysis (DDA) method. *Int J Rock Mech Min* 38(3):343–55
- Jones FO (1975) A laboratory study of the effects of confining pressure on fracture flow and storage capacity in carbonate rocks. *J Petrol Tech* 9(2):21–27
- Kazerani T, Yang ZY, Zhao J (2012) A discrete element model for predicting shear strength and degradation of rock joint by using compressive and tensile test data. *Rock Mech Rock Eng* 45(5):695–709
- Kim YI, Amadei B, Pan E (1999) Modeling the effect of water, excavation sequence and rock reinforcement with discontinuous deformation analysis. *Int J Rock Mech Min* 36(7):949–70
- Lemos JV, Lorig LJ (1990) Hydromechanical modeling of jointed rock masses using the distinct element method. In: Rossmann HJ (ed), Proc, 2nd International Conf on the Mechanics of Jointed and Faulted Rock, pp 605–611
- Li H, Li K, Subhash G, Kecskes LJ, Dowding RJ (2006) Micromechanical modeling of tungsten-based bulk metallic glass matrix composites. *Mater Sci EngA* 429:115–123
- Li X, Xu Q, Chen S (2016) An experimental and numerical study on water permeability of concrete. *Constr Build Mater* 105:503–510
- Lisjak A, Grasselli G (2014) A review of discrete modeling techniques for fracturing processes in discontinuous rock masses. *J Rock Mech Geotech Eng* 6(4):301–314
- McKee CR, Bumb AC, Koenig RA (1988). Stress-dependent permeability and porosity of coal and other geologic formations. *SPE Formation Eval* (1): 81–91
- Min KB, Jing LR (2003) Numerical determination of the equivalent elastic compliance tensor for fractured rock masses using the distinct element method. *Int J Rock Mech Min* 40(6):795–816
- Min KB, Rutqvist J, Tsang CF, Jing L (2004) Stress-dependent permeability of fractured rock masses: a numerical study. *Int J Rock Mech Min* 41(7):1191–1210
- Ni X, Chen W, Li Z, Gao X (2017) Reconstruction of different scales of pore-fractures network of coal reservoir and its permeability prediction with Monte Carlo method. *Int J Min Sci Tech* 27(4):693–699
- Nicksiar M (2013) Effective parameters on crack initiation stress in low porosity rocks. PhD thesis, Univ of Alberta, Edmonton
- Nygards M, Gudmundson P (2002) Micromechanical modeling of ferritic/pearlitic steels. *Mater Sci EngA* 325:435–443
- Wang HT (2000) Analysis of the stability of water-filled rock slope with fracture networks seepage and discrete element coupling. *Hydrogeol Eng Geol (China)* 27(2):30–33
- Wang JA, Park HD (2002) Fluid permeability of sedimentary rocks in a complete stress-strain process. *Eng Geol* 63(3/4):291–300
- Worthington PF (2008) A diagnostic approach to quantifying the stress sensitivity of permeability. *J Petrol Sci Eng* 61(2):49–57
- Wu YQ, Cao GZ, Ding WH (2005) Experimental study on relation between seepage and stress of sandstone in CT scale. *Chin J Rock Mech Eng* 23(24):4204–4209
- Xie HP, Chen ZD (1989) Analysis of rock fracture micro-mechanism. *J Chin Coal Soc* 2:57–67
- Yu J, Li H, Chen X (2013) Triaxial experimental study of associated permeability-deformation of sandstone under hydromechanical coupling. *Chin J Rock Mech Eng* 32(6):1204–1213
- Zhang C, Tu S, Zhang L (2016) A study on effect of seepage direction on permeability stress test. *Arab J Sci Eng* 41(11):1–14
- Zhang S, Tang SJ, Zhang DS, Fan G, Wang Z (2017) Determination of the height of the water-conducting fractured zone in difficult geological structures: a case study in Zhao Gu no. 1 coal seam. *Sustainability*. <https://doi.org/10.3390/su9071077>
- Zhu W, Wong TF (1997) The transition from brittle faulting to faulting to cataclastic flow: permeability evolution. *J Geophys Res* 102(B2):3027–3041